

Excitation spectra and correlation functions of quantum Su-Schrieffer-Heeger models

Manuel Weber, Fakher F. Assaad, and Martin Hohenadler

Institut für Theoretische Physik und Astrophysik, Universität Würzburg, 97074 Würzburg, Germany

(Dated: March 2, 2024)

We study one-dimensional Su-Schrieffer-Heeger (SSH) models with quantum phonons using a continuous-time quantum Monte Carlo method. Within statistical errors, we obtain identical results for the SSH model with acoustic phonons, and a related model with a coupling to an optical bond phonon mode. Based on this agreement, we first study the Peierls metal-insulator transition of the spinless SSH model, and relate it to the Kosterlitz-Thouless transition of a spinless Luttinger liquid. In the Peierls phase, the spectral functions reveal the single-particle and charge gap, and a central peak related to long-range order. For the spinful SSH model, which has a dimerized ground state for any nonzero coupling, we reveal a symmetry-related degeneracy of spin and charge excitations, and the expected spin and charge gaps as well as a central peak. Finally, we study the SSH-UV model with electron-phonon and electron-electron interaction. We observe a Mott phase with critical spin and bond correlations at weak electron-phonon coupling, and a Peierls phase with gapped spin excitations at strong coupling. We relate our findings to the extended Hubbard model, and discuss the physical origin of the agreement between optical and acoustic phonons.

PACS numbers: 71.10.Hf, 71.10.Pm, 71.30.+h

I. INTRODUCTION

In 1979, Su, Schrieffer and Heeger (SSH) introduced a simple microscopic model of polyacetylene with a modulation of the electronic hopping as a result of distortions of the carbon bonds [1]. It has since gained a much wider relevance due to the fact that it supports topological excitations (solitons) with fractional charge [1–3], and its relation to one-dimensional topological insulators [4] in the BDI class [5]. As a model for correlated electrons, the case of a half-filled band has attracted particular interest, because it supports a Peierls and (in the presence of Coulomb interaction) a Mott insulating phase. If the lattice is treated quantum mechanically, the model constitutes a rich and complex many-body problem.

In the adiabatic limit (or at the mean-field level), a dimerized Peierls state results at $T = 0$ for any nonzero electron-phonon coupling [1, 6]. Although a classical treatment of the lattice (see, e.g., Refs. [7–9]) appears justified for polyacetylene given the large oscillator mass [1], quantum fluctuations of the lattice cause a significant reduction of the dimerization [6, 10–13] and affect the low-lying excitations [14]. Quite surprisingly, numerical [6, 10, 15] and analytical [6, 16–18] results for the SSH model without electron-electron interaction suggest that lattice fluctuations do not destroy the Peierls state, in contrast to the spinless SSH model [6] or Holstein models [19–21]. Interestingly, the Peierls state does become unstable with respect to quantum fluctuations if additional Coulomb repulsion between electrons is taken into account, as appropriate for polyacetylene [22]. In fact, the single-particle gap found experimentally has been argued to be predominantly a result of electronic correlations, with only a small component from the dimerization of the lattice [7]. A finite phonon frequency may also crucially affect the balance between interactions [23, 24]. The SSH models are also related to spin-Peierls models

[6, 25], studied in detail to understand the physics of CuGeO_3 [26], see for example Refs. [27, 28]. For a more complete overview of previous work on polyacetylene we refer to Refs. [22, 29].

The momentum dependence of the phonon dispersion and the interaction make numerical studies of the SSH model more challenging than for models with a Holstein interaction [30]. Therefore, several open problems remain, in particular the calculation of momentum-resolved excitation spectra. Besides, some of the recent numerical work has focused on a simplified model with optical phonons and a different interaction term [25]. While theory suggests that the low-energy physics depends solely on the phonon frequency at $q = 2k_F$ [6, 16], the quantitative impact of the phonon dispersion is not fully understood. In particular, recent functional renormalization group results for the model with acoustic phonons [18] agree quantitatively with numerical results for the model with optical phonons [25]. On the other hand, a significant effect of the dispersion was reported in Ref. [31].

Here, we use quantum Monte Carlo simulations of the original SSH model (with acoustic phonons) to demonstrate that it gives results that are identical within statistical errors to the simplified model with optical phonons for all parameters considered. Given this agreement, we study in detail the real-space correlation functions and calculate spectral functions of the simplified models. We consider the spinless and the spinful SSH model, as well as the SSH model with additional Coulomb interaction.

The paper is organized as follows. In Sec. II we define the models, in Sec. III we discuss the key methodological aspects, in Sec. IV we present the numerical results, in Sec. V we discuss the impact of the phonon dispersion and lattice fluctuations as well as the low-energy theory, and in Sec. VI we conclude.

II. MODELS

In addition to the original SSH model [1], two other variants have been studied in the past. First, an SSH model with optical phonons but with the original coupling term, proposed in Ref. [32], and second a model with optical phonons and a simplified coupling term introduced in Ref. [25].

A. SSH model

Defining the bond operator

$$\hat{B}_i = \sum_{\sigma} \left(\hat{c}_{i\sigma}^{\dagger} \hat{c}_{i+1\sigma} + \hat{c}_{i+1\sigma}^{\dagger} \hat{c}_{i\sigma} \right) \quad (1)$$

the SSH Hamiltonian [1] can be written as

$$\begin{aligned} \hat{H} = & -t \sum_i \hat{B}_i + g \sum_i \hat{B}_i (\hat{Q}_{i+1} - \hat{Q}_i) \\ & + \sum_i \left[\frac{1}{2M} \hat{P}_i^2 + \frac{K}{2} (\hat{Q}_{i+1} - \hat{Q}_i)^2 \right]. \end{aligned} \quad (2)$$

The first term describes nearest-neighbor electronic hopping with amplitude t in the undistorted chain, the second term is a coupling between electrons and phonons in the form of a modulation of the electronic hopping as a result of lattice distortions (see also Ref. [33]), and the last term describes harmonic oscillators with mass M , spring constant K , coordinate \hat{Q}_i , and momentum \hat{P}_i ; it can be written as $\sum_q \omega_q \hat{b}_q^{\dagger} \hat{b}_q$, with the phonon dispersion $\omega_q = \omega_{\pi} \sin(q/2)$.

The spinless SSH model has the same form as Eq. (2), with the bond operator given by $\hat{B}_i = \hat{c}_i^{\dagger} \hat{c}_{i+1} + \hat{c}_{i+1}^{\dagger} \hat{c}_i$ [6].

B. Optical SSH model

We also simulated the Hamiltonian [25]

$$\hat{H} = -t \sum_i \hat{B}_i + \sum_i \left[\frac{1}{2M} \hat{P}_i^2 + \frac{K}{2} \hat{Q}_i^2 \right] + g \sum_i \hat{B}_i \hat{Q}_i, \quad (3)$$

which describes the coupling of electrons to optical phonons with frequency $\omega_0 = \sqrt{K/M}$. As in the SSH model, lattice distortions modulate the electronic hopping, but the interaction only involves the coordinate \hat{Q}_i rather than the difference $\hat{Q}_{i+1} - \hat{Q}_i$. In the following, we refer to Eq. (3) as the optical SSH model, and will demonstrate that it gives the same results as the SSH model (2). The optical phonons in Eq. (3) may be regarded as describing fluctuations of the bonds rather than atom positions as in Eq. (2). As discussed in Sec. V, this interpretation provides a physical understanding of the observed agreement between Eqs. (2) and (3).

C. SSH-UV model

In the spinful case, we will also study the impact of electron-electron interactions. Following previous work [7, 23, 25, 31, 34], we considered onsite and nearest-neighbor repulsion, as described by

$$\hat{H}_{\text{ee}} = U \sum_i \left(\hat{n}_{i\uparrow} - \frac{1}{2} \right) \left(\hat{n}_{i\downarrow} - \frac{1}{2} \right) + V \sum_i (\hat{n}_i - 1) (\hat{n}_{i+1} - 1), \quad (4)$$

with $\hat{n}_i = \hat{n}_{i\uparrow} + \hat{n}_{i\downarrow}$. We have simulated Eq. (4) in combination with the original SSH model (2) (SSH-UV model) and the simplified model (3) (optical SSH-UV model).

D. Spin-charge symmetry

For our choice of zero chemical potential $\mu = 0$, and on bipartite lattices, the models (2) and (3) are invariant under the particle-hole transformation $\hat{c}_{i(\sigma)} \mapsto (-1)^i \hat{c}_{i(\sigma)}^{\dagger}$, and hence half-filled. For $U = V = 0$, the spinful SSH and optical SSH models are furthermore invariant under $\hat{c}_{i\downarrow} \mapsto (-1)^i \hat{c}_{i\downarrow}^{\dagger}$ [19], which interchanges spin and charge degrees of freedom. Whereas this transformation maps the repulsive to the attractive Hubbard model [35], here it implies a perfect degeneracy of spin and charge degrees of freedom for $U = V = 0$, as confirmed by our results.

E. Conventions

We focus on half-filling, corresponding to an average density $\langle \hat{n}_i \rangle = 1$ for the spinful case, and to $\langle \hat{n}_i \rangle = 0.5$ for the spinless case. We use t as the unit of energy, and set the lattice constant and \hbar to one. We define the dimensionless coupling constant $\lambda = g^2/Kt$, and consider chains with L sites and periodic boundary conditions. The inverse temperature was chosen as $\beta t = L$.

III. METHOD

We used the continuous-time interaction-expansion (CT-INT) quantum Monte Carlo method, which is based on a weak-coupling expansion of the partition function, and gives exact results for finite systems [36].

We write the SSH model (2) in the generic form

$$\hat{H} = \hat{H}_0 + \sum_q \omega_q \hat{b}_q^{\dagger} \hat{b}_q + \gamma \sum_q (\hat{\rho}_q \hat{b}_q^{\dagger} + \hat{\rho}_q^{\dagger} \hat{b}_q) \quad (5)$$

with the charge operator

$$\hat{\rho}_q = \frac{2i}{\sqrt{L}} \frac{1}{\sqrt{2M\omega_q}} \sum_{k\sigma} \hat{c}_{k\sigma}^{\dagger} \hat{c}_{k+q\sigma} [\sin k - \sin(k+q)]. \quad (6)$$

The partition function takes the form

$$Z = \int D(\bar{\psi}, \psi) e^{-S_0[\bar{\psi}, \psi]} \int D(\bar{\phi}, \phi) e^{-S_{\text{ep}}[\bar{\psi}, \psi, \bar{\phi}, \phi]}. \quad (7)$$

Here, S_0 describes the noninteracting fermions, whereas the phonon and electron-phonon contributions to Eq. (2) are contained in S_{ep} . Carrying out the Gaussian integrals over the phonon degrees of freedom [37, 38] gives a retarded and nonlocal electron-electron interaction

$$S_1 = -\frac{g^2}{2K} \iint_0^\beta d\tau d\tau' \sum_{ij} B_i(\tau) \Gamma(i-j, \tau - \tau') B_j(\tau'), \quad (8)$$

where $\Gamma(r, \tau) = L^{-1} \sum_q e^{-iqr} D(q, \tau)$ and

$$D(q, \tau) = \frac{\omega_q}{2} \frac{\cosh[\omega_q(|\tau| - \beta/2)]}{\sinh[\omega_q\beta/2]}. \quad (9)$$

A similar representation of the phonon-mediated interaction was given in Ref. [6]; however, in the continuum approximation, the SSH interaction becomes local in space, as characteristic of Holstein models [30].

For the optical SSH model, the interaction reduces to

$$S_1 = -\frac{g^2}{2K} \iint_0^\beta d\tau d\tau' \sum_i B_i(\tau) D(\tau - \tau') B_i(\tau'), \quad (10)$$

where $D(\tau)$ follows from Eq. (9) by replacing $\omega_q \mapsto \omega_0$. Although both bond operators in Eq. (10) carry the same index i , the interaction remains nonlocal because $B_i(\tau)$ involves the sites i and $i+1$.

The interactions described by Eqs. (8) and (10) can be simulated with the CT-INT method by implementing a general vertex with four lattice indices, two time indices, and two spin indices. For the optical SSH models, there is no sign problem so that a sampling over additional Ising spins [38] is not necessary.

In the case of the SSH-UV model, the additional Coulomb interaction described by Eq. (4) enters the partition function in the form of

$$S_2 = U \int_0^\beta d\tau \sum_i [n_{i\uparrow}(\tau) - \frac{1}{2}][n_{i\downarrow}(\tau) - \frac{1}{2}] \quad (11)$$

$$+ V \int_0^\beta d\tau \sum_i \sum_{\sigma\sigma'} [n_{i\sigma}(\tau) - \frac{1}{2}][n_{i+1\sigma'}(\tau) - \frac{1}{2}].$$

The implementation of such interactions within the CT-INT method, including the use of auxiliary Ising fields to avoid a sign problem, has been discussed in Refs. [38, 39]. The simultaneous sampling of the interactions S_1 and S_2 is done by randomly choosing a vertex type.

The numerical effort scales as $(\alpha\beta L)^3$ with $\alpha \sim \lambda$ for $U = V = 0$, and $\alpha \sim U$ for $U \gg V, \lambda$.

A. Sign problem

Previous applications of the CT-INT method to electron-phonon models only considered the case of optical phonons. For the SSH model, the momentum dependence of the phonon dispersion ω_q leads to a pronounced minus sign problem whose origin can be traced back to the fact that $\Gamma(r, \tau)$ (and hence the configuration weight) can take on negative values for $r > 0$ in the case of dispersive phonons. The sign problem can be improved to some extent (at the expense of a higher expansion order) by generalized offsets $\alpha(\tau, s)$ (depending on Ising spins $s = \pm 1$, cf. Ref. [38]) in the bond operators $B_i(\tau)$ for vertices with negative weight.

B. Observables

We calculated the real-space correlation functions

$$C_b(r) = \langle (\hat{B}_r - b)(\hat{B}_0 - b) \rangle \quad (\text{bond}) \quad (12)$$

$$C_\rho(r) = \langle (\hat{n}_r - n)(\hat{n}_0 - n) \rangle \quad (\text{charge}) \quad (13)$$

$$C_\sigma(r) = \langle \hat{s}_r^x \hat{s}_0^x \rangle \quad (\text{spin}) \quad (14)$$

$$C_p(r) = \langle \hat{\Delta}_r^\dagger \hat{\Delta}_0 \rangle \quad (\text{pairing}) \quad (15)$$

Here, $n = \langle \hat{n}_i \rangle$, $b = \langle \hat{B}_i \rangle$, and we consider the transverse spin correlations ($\langle \hat{s}_r^x \hat{s}_0^x \rangle$ is identical within error bars to $\langle \hat{s}_r^z \hat{s}_0^z \rangle$, as required by symmetry). The pairing operator $\hat{\Delta}_r$ is defined as $\hat{\Delta}_r = c_{r\uparrow}^\dagger c_{r\downarrow}^\dagger$ for spinful fermions (singlet pairing), and as $\hat{\Delta}_r = c_{r\uparrow}^\dagger c_{r+1}^\dagger$ for spinless fermions (extended singlet pairing).

In combination with the maximum entropy method [40], we calculated the single-particle spectral function

$$A(k, \omega) = \frac{1}{Z} \sum_{ij} |\langle i | \hat{O}_k | j \rangle|^2 (e^{-\beta E_i} + e^{-\beta E_j}) \delta(\Delta_{ji} - \omega), \quad (16)$$

with $\hat{O}_k = c_k$ for spinless fermions, and $\hat{O}_k = c_{k\sigma}$ for spinful fermions. Additionally, we calculated

$$S_\alpha(q, \omega) = \frac{1}{Z} \sum_{ij} |\langle i | \hat{O}_q^\alpha | j \rangle|^2 e^{-\beta E_i} \delta(\Delta_{ji} - \omega), \quad (17)$$

with \hat{O}_q^α either a bond, charge, or spin operator. Here, $|i\rangle$ is an eigenstate with energy E_i , and $\Delta_{ji} = E_j - E_i$.

IV. RESULTS

A. SSH model vs. optical SSH model

Several different SSH-type models have been studied in the literature. The phase diagram for a half-filled band has been investigated numerically in terms of the original Hamiltonian (2) in Ref. [6] (with a cutoff to avoid an

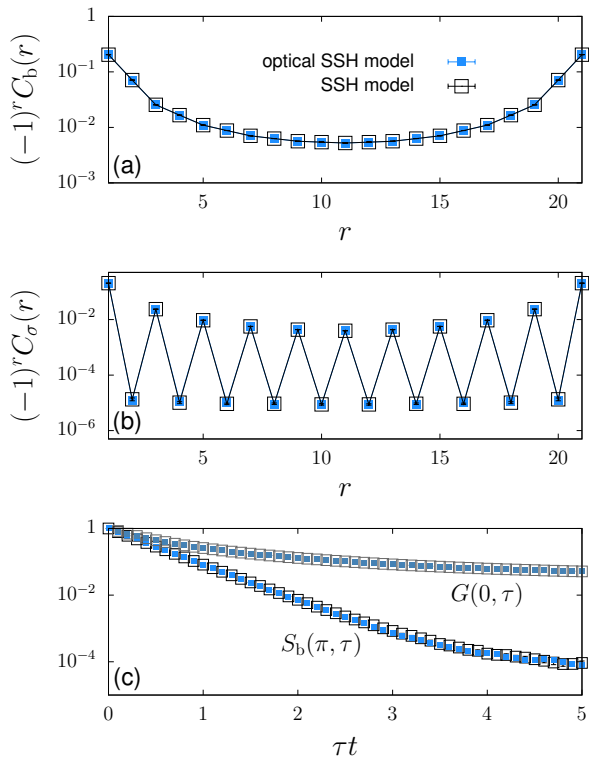


FIG. 1. (Color online) Comparison between the optical SSH model (filled symbols) and the SSH model (open symbols) for (a) real-space bond correlations, (b) real-space spin correlations, (c) the single-particle Green function $G(k=0, \tau)$ and the dynamic bond correlation function $S_b(q=\pi, \tau)$. Here, $\beta t = L = 22$, $\omega_0 = \omega_\pi = 0.1t$, $U = V = 0$, and $\lambda = 0.2$.

unphysical sign change of the hopping term for large distortions), in Ref. [15] by solving the original SSH model, in Ref. [25] by considering the optical SSH model (3), and in Ref. [31] by simulating the original interaction term in combination with a general phonon dispersion and extrapolating to acoustic and optical phonons [31].

Here, we present a comparison of the SSH model (2) and the optical SSH model (3), taking $\omega_0 = \omega_\pi = 0.1t$ to alleviate the sign problem; a larger value $\omega_0 = \omega_\pi = 0.5t$ was used for most other results. Figure 1(a) shows the bond correlation function $C_b(r)$, whereas Fig. 1(b) shows the corresponding spin correlations. Remarkably, the results for the models (2) and (3) are identical within statistical errors. This quantitative agreement also extends to dynamic correlation functions, as demonstrated for the single-particle Green function at momentum $k=0$ and the dynamic bond correlation function at $q=\pi$ in Fig. 1(c). In addition to the results shown in Fig. 1, we compared bond, charge, spin, and pairing correlation functions, as well as the momentum distribution function, for several other parameter sets, including nonzero U and V , higher temperatures, stronger coupling, and spinless models. All results were identical within error bars to those for the original SSH coupling and acoustic phonons. Based on this agreement, whose origin will be

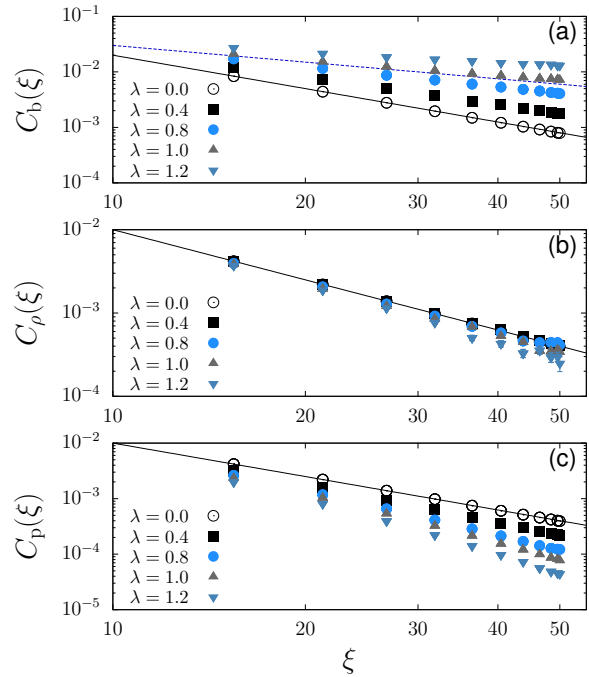


FIG. 2. (Color online) (a) Bond, (b) charge, and (c) pairing correlations of the spinless optical SSH model as a function of $\xi = L \sin(\pi r/L)$ (see text). Here, $\beta t = L = 50$, and $\omega_0 = 0.5t$. The solid lines correspond to $1/r^2$, the dashed line corresponds to $1/r$. Here and in Figs. 6 and 11, the correlation functions are plotted only for odd distances r .

discussed in Sec. V, we avoided the sign problem by simulating the corresponding sign-free optical SSH models.

B. Spinless fermions

Given the theoretical prediction of an extended metallic phase without long-range bond order in the spinless SSH model [6], we show in Fig. 2 the real-space bond, charge, and pairing correlation functions defined in Sec. III. To eliminate boundary effects, we use the conformal distance $\xi = L \sin(\pi r/L)$ [41]. This allows us to directly compare to the bosonization results for a spinless Luttinger liquid [42, 43]

$$\begin{aligned}
 C_b(r) &= \frac{A_b}{r^{2K_\rho}} \cos(2k_F r), \\
 C_\rho(r) &= -\frac{K_\rho}{2\pi^2 r^2} + \frac{A_\rho}{r^{2K_\rho}} \cos(2k_F r), \\
 C_p(r) &= \frac{A_p}{r^{2K_\rho^{-1}}}.
 \end{aligned} \tag{18}$$

For $\lambda = 0$, all correlators decay with a power law $1/r^2$. According to our results, bond correlations become dominant for $\lambda > 0$, suggesting $K_\rho < 1$ and hence a repulsive Luttinger liquid, in accordance with Ref. [17]. At the same time, charge and pairing correlations are suppressed. While the decay of pairing correlations can be

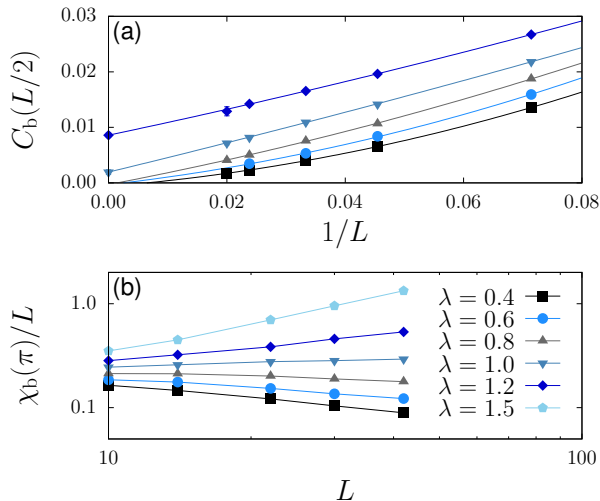


FIG. 3. (Color online) (a) Finite-size scaling of the bond correlations at the largest distance $r = L/2$, using a second-order polynomial extrapolation. (b) Finite-size scaling of the bond susceptibility for the spinless optical SSH model. Here, $\beta t = L$, and $\omega_0 = 0.5t$. The key in (b) applies to both panels.

explained by the increase of the exponent $2K_\rho^{-1}$, $2k_F$ charge correlations formally have the same exponent as $2k_F$ bond correlations, see Eq. (18). The absence of enhanced charge correlations in Fig. 2(b) can be attributed to a suppression of the amplitude, $A_\rho \rightarrow 0$ [44], causing the first term ($1/r^2$) to dominate in the metallic phase [the exponent is close to 2 in Fig. 2(b)]. Pairing correlations [Fig. 2(c)] are always subdominant in the metallic phase. In the insulating phase, charge and pairing correlations are strongly suppressed—consistent with an exponential decay—while bond correlations become long-ranged.

To determine the critical value λ_c for the Peierls transition, we show in Fig. 3(a) a finite-size scaling of the bond correlations at the largest distance $r = L/2$. The extrapolation using system sizes up to $L = 50$ suggests $\lambda_c = 0.9(1)$. The onset of long-range order can also be tracked by calculating the bond susceptibility [25]

$$\chi_b(\pi) = \frac{1}{L} \sum_{ij} (-1)^{i-j} \int_0^\beta d\tau \langle \hat{B}_i(\tau) \hat{B}_j(0) \rangle. \quad (19)$$

As a function of L (and for $\beta = L$), $\chi_b(\pi)/L$ is expected to vanish in the metallic phase, and to diverge $\sim L$ in the dimerized Peierls phase. For spinless fermions, χ_b has a more favorable scaling with system size than the bond correlations shown in Fig. 3(a), and does not involve an unknown scaling function. Our numerical results in Fig. 3(b) confirm the expected behavior of the susceptibility, and give a critical value consistent with Fig. 3(a). We also carried out simulations for other phonon frequencies, and found that λ_c increases with increasing ω_0 , in agreement with theoretical expectations [6].

Within a bosonization description of the Luttinger liq-

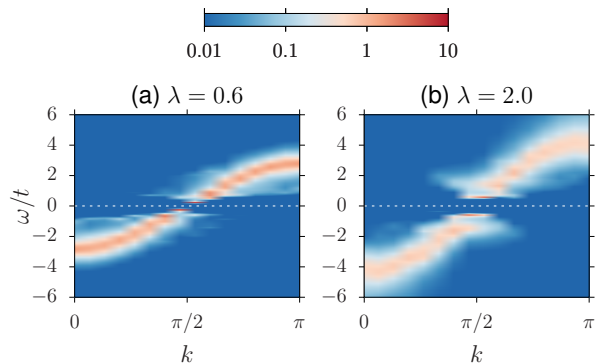


FIG. 4. (Color online) Single-particle spectral function $A(k, \omega)$ of the spinless optical SSH model. The dashed line indicates the Fermi level. Here, $\beta t = L = 30$, $\omega_0 = 0.5t$. Color scheme for this and other density plots from Ref. [47].

uid to (charge-density-wave) insulator transition, $K_\rho = 1/2$ corresponds to the critical point of the Kosterlitz-Thouless phase transition. Equation (18) therefore suggests a $1/r$ decay at the critical point. Although we have to consider the possibility of logarithmic corrections in the vicinity of the transition, the correlation functions in Fig. 2(a) indeed decay slightly faster than $1/r$ (consistent with $K_\rho > 1/2$) for $\lambda = 0.8$, and slightly slower than $1/r$ for $\lambda = 1$, consistent with $\lambda_c = 0.9(1)$.

To further characterize the two phases, we calculated spectral functions. Figure 4 shows the single-particle spectral function for (a) $\lambda = 0.6$ (metallic phase) and (b) $\lambda = 2$ (insulating phase). In Fig. 4(a) we see a gapless (within the available momentum resolution) band derived from the bare dispersion $-2t \cos k$. The most prominent effects of the electron-phonon coupling are (i) a substantial broadening outside the coherent interval $[-\omega_0, \omega_0]$, and (ii) an enhanced bandwidth [$\approx 6t$ in Fig. 4(a)] arising from the enhanced hopping due to the SSH interaction, see Eq. (3). (The bandwidth of the spectrum remains $\approx 4t$ in Holstein-type models [45].) In the Peierls phase, Fig. 4(b), the spectrum has acquired a gap at the Fermi level, and exhibits signatures of backfolded shadow bands characteristic of systems with reduced periodicity [46]. While these features are qualitatively captured by mean-field theory [45], at and near k_F , we can identify two separate energy scales in Fig. 4(b) previously discussed for the spinless Holstein model [45]. The lowest-energy excitation can be related to soliton excitations [45], whereas the high-energy excitations correspond to the renormalized cosine band structure with a dimerization gap.

Figure 5 shows the corresponding dynamic bond and density structure factors. For weak coupling, the latter still resemble the noninteracting particle-hole continuum. Additionally, the bond structure factor in Figs. 5(a) and (b) reveals at low energies the renormalized phonon frequency, in particular a central ($\omega = 0$) peak at $q = \pi$ in the Peierls phase in Fig. 5(b) related to long-range order (in the Holstein model, where the lattice is cou-

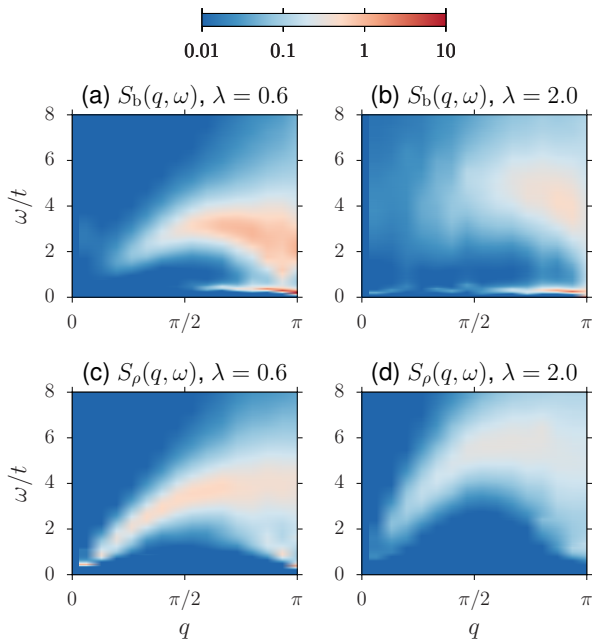


FIG. 5. (Color online) (a)–(b) Dynamic bond and (c)–(d) dynamic density structure factor of the spinless optical SSH model. Here, $\beta t = L = 30$, and $\omega_0 = 0.5t$.

pled to the charge, the phonon dispersion appears in the dynamic charge structure factor [45, 48]). The density structure factor in the metallic phase, Fig. 5(c), features a gapless linear mode at small q , whereas a gap and a strong suppression of low-energy excitations are visible in the Peierls phase, see Fig. 5(d).

C. Spinful fermions

We begin by considering the real-space correlation functions shown in Fig. 6. Similar to the spinless case, bond correlations decay increasingly slowly upon switching on the electron-phonon coupling. At the same time, we observe a suppression of charge, pairing and spin correlations [spin correlations are shown in Fig. 6(b), the others behave similarly]. Since we expect an ordered Peierls state for any $\lambda > 0$, bond correlations should oscillate with a constant, nonzero amplitude at large distances, and all other correlation functions should decay exponentially. While the finite-size extrapolation of the bond correlations at the largest distance in Fig. 7(a) gives a nonzero value already for $\lambda = 0.2$, the expected exponential decay of spin correlations is only clearly visible (for the system size used) for $\lambda = 0.6$ in Fig. 6(b).

The Peierls state can be detected even at weak coupling. Because the bond susceptibility is not a reliable indicator to track the onset of long-range order in systems with a spin gap [49], we instead consider the finite-size estimates of the Luttinger liquid parameters K_ρ and K_σ . The latter are defined in terms of the charge and spin

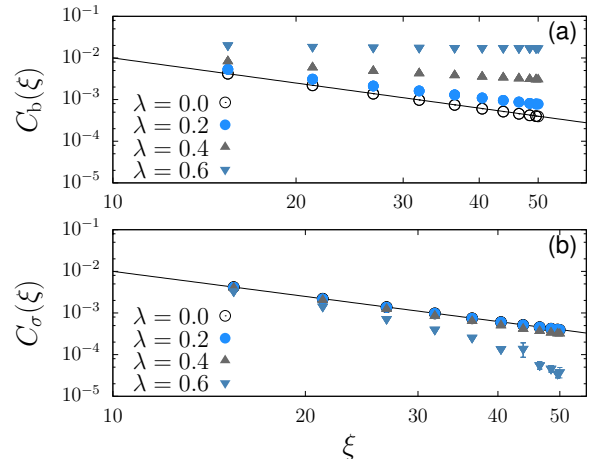


FIG. 6. (Color online) (a) Bond and (b) spin correlations of the spinful optical SSH model as a function of $\xi = L \sin(\pi r/L)$. Here, $\beta t = L = 50$, and $\omega_0 = 0.5t$. The solid lines correspond to $1/r^2$

structure factors as

$$\begin{aligned} K_\rho(L) &= \pi S_\rho(q_1)/q_1, \\ K_\sigma(L) &= \pi S_\sigma(q_1)/q_1, \end{aligned} \quad (20)$$

where $q_1 = 2\pi/L$ is the smallest nonzero wave vector for system size L . Finite-size extrapolation has been shown to give accurate results for the Luttinger parameters, for example, in the extended Hubbard model [50]. However, as argued in Refs. [25, 51], even very small spin gaps can be detected from values $K_\sigma(L) < 1$, as they imply $K_\sigma(L \rightarrow \infty) = 0$. In contrast, in systems with gapless spin excitations, numerical simulations usually give $K_\sigma(L) > 1$ with a very slow (logarithmic) convergence to the value $K_\sigma = 1$ implied by the $SU(2)$ spin symmetry. This diagnostic gives reliable results for the integrable attractive and repulsive Hubbard models [52]. For the SSH model, we find $K_\sigma(L) < 1$ and hence a spin gap even for $\lambda = 0.1$ [Fig. 7(b)], which is consistent with a Peierls state for any $\lambda > 0$. The same behavior is observed over the whole range of phonon frequencies from the adiabatic to the antiadiabatic regime, see Fig. 7(c).

In general, a spin gap does not necessarily imply long-range Peierls order. For example in the Holstein model, an extended metallic (Luther-Emery [53]) phase with a spin gap but gapless charge excitations [54] exists. While theory suggests that the spin and charge gaps open simultaneously in the SSH model, we can obtain explicit evidence from the degeneracy of $K_\rho(L)$ and $K_\sigma(L)$ in Fig. 7(b). Within statistical errors, the correlation functions $S_\rho(q, \tau)$ and $S_\sigma(q, \tau)$ and hence also $K_\rho(L)$ and $K_\sigma(L)$ are identical. This is a consequence of the spin-charge symmetry discussed in Sec. II, and has important consequences: if $K_\sigma(L) < 1$ indicates a spin gap, $S_\rho(q, \tau) = S_\sigma(q, \tau)$ implies also a charge gap and hence insulating behavior. Figure 7(b) therefore suggests that

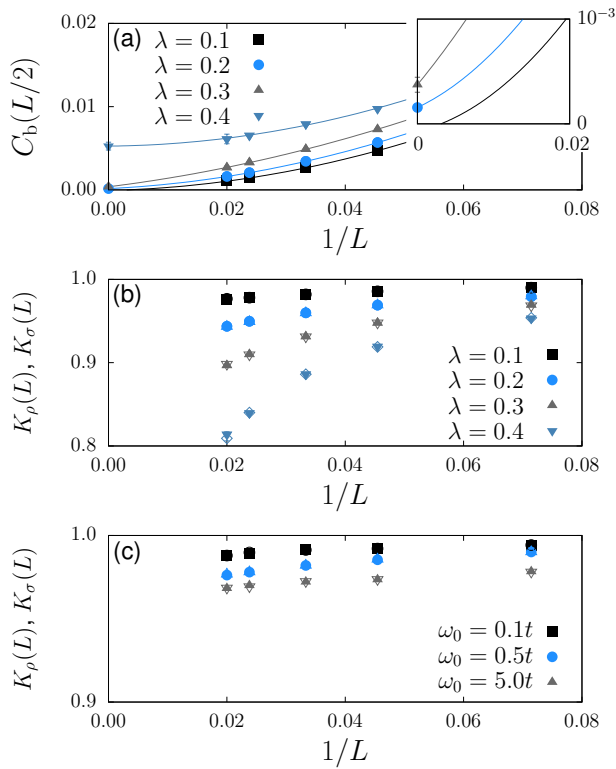


FIG. 7. (Color online) (a) Finite-size scaling of the bond correlations at the largest distance $r = L/2$ for the spinful optical SSH model and different values of λ . Here, $\beta t = L$, and $\omega_0 = 0.5t$. The inset shows a closeup of the extrapolated values. (b) Finite-size estimates of the Luttinger liquid parameters [we find $K_\rho(L) = K_\sigma(L)$ within error bars] for the same parameters as in (a). (c) $K_\rho(L)$ and $K_\sigma(L)$ for different phonon frequencies. Here, $\beta t = L$, and $\lambda = 0.1$.

the spinful optical SSH model is a Peierls insulator even for very small λ , in agreement with the theoretical prediction of $\lambda_c = 0$. Given the quantitative agreement between the optical SSH model and the SSH model demonstrated in Fig. 1, our findings carry over to Eq. (2).

Having established the insulating behavior for any $\lambda > 0$, we now consider excitation spectra. Figure 8 shows the single-particle spectral function for $\lambda = 0.6$ and $\lambda = 1$. The gap opens exponentially starting from $\lambda = 0$. Nevertheless, we see a small gap and backfolded shadow bands in Fig. 8(a), in contrast to the results for the metallic phase of the spinless model in Fig. 4(a) for the same value of the coupling ($\lambda = 0.6$). For a stronger coupling $\lambda = 1$, Fig. 8(b) reveals a substantial gap, and the spectrum closely resembles that of the spinless SSH model in the Peierls phase, see Fig. 4(b).

Figure 9 shows the dynamic bond and spin structure factors for $\lambda = 1$. As expected for the dimerized phase, Fig. 9(a) features a central peak with large spectral weight at $q = \pi$. Both charge and spin excitations (identical within error bars) are gapped at small q .

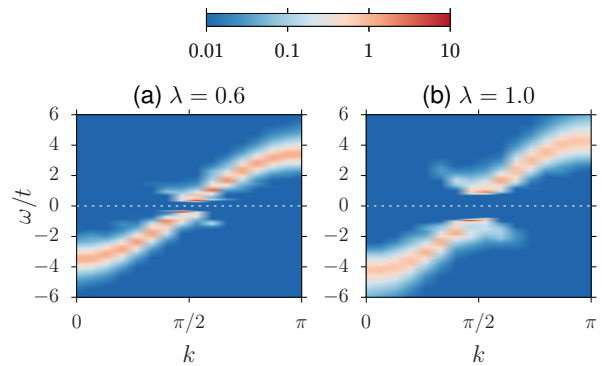


FIG. 8. (Color online) Single-particle spectral function $A(k, \omega)$ of the spinful optical SSH model. The dashed line indicates the Fermi level. Here, $\beta t = L = 30$, and $\omega_0 = 0.5t$.

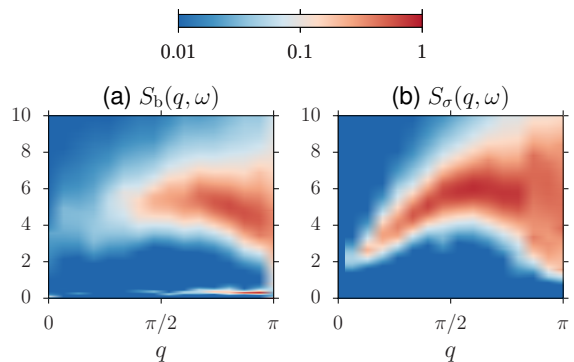


FIG. 9. (Color online) (a) Dynamic bond and (b) dynamic spin structure factor of the spinful optical SSH model. Here, $\beta t = L = 30$, $\omega_0 = 0.5t$, and $\lambda = 1$.

D. Spinful fermions with Coulomb interaction

We now turn to the spinful SSH-UV model with $U = 4V = 2.5t$, considered to be appropriate for polyacetylene [7], and a phonon frequency $\omega_0 = 0.5t$. In principle, our method can also be applied to models with long-range interactions [55]. Because Eqs. (2) and (3) give identical results even with the additional electron-electron interaction, we simulated the optical SSH model to avoid the minus-sign problem mentioned in Sec. III.

From Refs. [25, 31, 56], it is known that the phase diagram consists of Mott and Peierls insulating regions, except for the adiabatic limit where the Peierls state seems to remain stable for any $\lambda > 0$. Away from this limit, the system is a Mott insulator for $\lambda < \lambda_c$, with gapless spin excitations but a gap for single-particle and charge excitations. For $\lambda = 0$ (extended Hubbard model), the ground state is a Mott insulator for $U \gg 2V$ [44, 51, 57], as relevant for polyacetylene. The electron-phonon coupling competes with the dominant antiferromagnetic spin correlations, and eventually gives rise to a Peierls phase with a spin gap and long-range bond order [25, 31].

To estimate λ_c for the Mott-Peierls transition for our

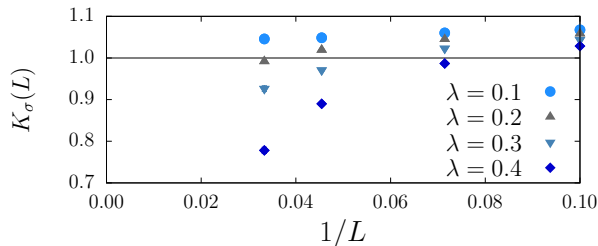


FIG. 10. (Color online) Finite-size scaling of $K_\sigma(L)$ for the optical SSH-UV model. Here, $\beta t = L$, $\omega_0 = 0.5t$, $U = 2.5t$, and $V = 0.625t$.

choice of parameters, we carried out a finite-size scaling of $K_\sigma(L)$; the additional Coulomb interaction restricts us to system sizes $L \leq 30$. The results in Fig. 10 for $\lambda = 0.1$ are consistent with the absence of a spin gap and $K_\sigma = 1$, and therefore with a Mott insulating state. In contrast, for $\lambda \geq 0.2$, we have $K_\sigma(L) < 1$ and a finite-size dependence consistent with $K_\sigma = 0$ and a spin-gapped Peierls phase. Moreover, we find $K_\rho(L) < 1$ for all values of λ considered, and a very weak dependence of $K_\rho(L)$ on λ in the range $0 \leq \lambda \leq 0.4$ (not shown).

Figure 11 shows the real-space correlation functions for bond, spin, charge and pairing operators in the Mott ($\lambda = 0.1$) and the Peierls phase ($\lambda = 0.4$), respectively. Because the system has a charge gap in both phases, the charge and pairing correlations (see Ref. [42] for the explicit Luttinger liquid results) in general decay exponentially; the former because $K_\rho = 0$ and $A_\rho \rightarrow 0$, similar to the spinless case, the latter because the exponents diverge for $K_\rho = 0$. Figures 11(c) and 11(d) reveal a strong suppression compatible with an exponential decay. For nonzero U and V , the SSH-UV model is no longer invariant under the modified particle-hole transformation, and the degeneracy of spin and charge correlations is lifted.

The bond and spin correlations are more interesting. In a Luttinger liquid, their $2k_F$ components decay as [58]

$$\begin{aligned} C_b^{2k_F}(r) &= \frac{A_b}{r^{K_\rho + K_\sigma}} \cos(2k_F r), \\ C_\sigma^{2k_F}(r) &= \frac{A_\sigma}{r^{K_\rho + K_\sigma^{-1}}} \cos(2k_F r), \end{aligned} \quad (21)$$

where we neglected potential logarithmic corrections due to marginal operators. In the Mott phase with $K_\rho = 0$ and $K_\sigma = 1$ (corresponding to a Luttinger liquid in the spin sector, or COS1 in the notation of Ref. [59]), Eq. (21) predicts a $1/r$ decay, in good agreement with our results in Fig. 11(a) and 11(b). While we cannot exclude logarithmic corrections on the accessible system sizes, our results are consistent with a larger amplitude for spin correlations than for bond correlations, $A_\sigma > A_b$. In the Peierls phase ($K_\rho = K_\sigma = 0$, COS0), bond correlations become long-ranged and spin correlations decay exponentially as a result of the nonzero spin gap, see Fig. 11.

Although finite values of U , V give rise to a Mott phase for small enough λ , it has been observed that $2k_F$

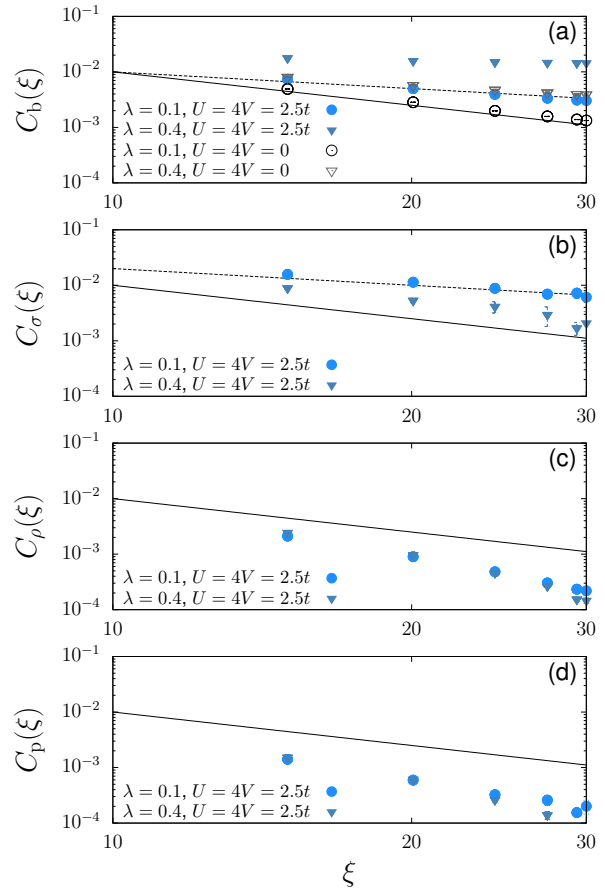


FIG. 11. (Color online) (a) Bond, (b) spin, (c) charge, and (d) pairing correlations of the optical SSH-UV model as a function of $\xi = L \sin(\pi r/L)$. The solid (dashed) line illustrates a $1/r^2$ (a $1/r$) decay. Here, $\beta t = L = 30$, $\omega_0 = 0.5t$, $U = 2.5t$, and $V = 0.625t$.

bond correlations are actually enhanced by Coulomb interactions [23, 24, 34, 60]. Our results in Fig. 11(a) confirm such an enhancement. Interestingly, previous work showed that the power-law exponent of $2k_F$ bond correlations is independent of U and V [24], namely equal to one in the Mott phase and zero in the Peierls phase; the data in Fig. 11(a) are compatible with this result. The enhancement of bond correlations is therefore related to a larger amplitude A_b . While A_σ grows continuously with increasing U , A_b has been found to have a maximum near $U \sim 4t$ [23, 24, 34, 56].

Figure 12 shows the single-particle spectral function for $\lambda = 0.1$ [Mott phase, Fig. 12(a)] and $\lambda = 0.4$ [Peierls phase, Fig. 12(b)]. In both cases, we find a gap at the Fermi level that increases with increasing λ . Moreover, the SSH electron-phonon coupling again gives rise to an enhanced bandwidth of the cosine-like band. For intermediate values near the Mott-Peierls transition (not shown), we find no evidence for a closing of the gap, consistent with an insulator-insulator transition without an intermediate metallic state.

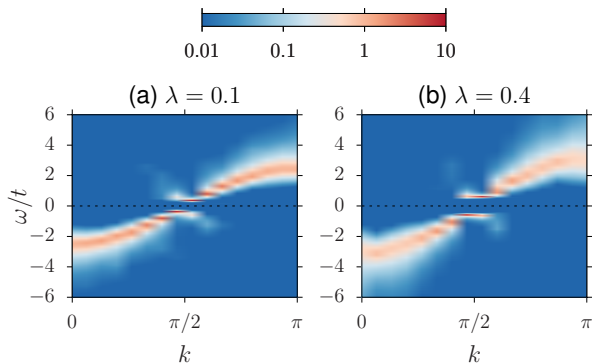


FIG. 12. (Color online) Single-particle spectral function $A(k, \omega)$ of the optical SSH-UV model. The dashed line indicates the Fermi level. Here, $\beta t = L = 30$, $\omega_0 = 0.5t$, $U = 2.5t$, and $V = 0.625t$.

In Fig. 13, we present the two-particle excitation spectra in the Mott phase ($\lambda = 0.1$) and the Peierls phase ($\lambda = 0.4$). Whereas only a partial softening of the phonon mode at $q = \pi$ is visible in the structure factor in the Mott phase [Fig. 13(a)], we observe a central peak at $q = \pi$ in the Peierls phase [Fig. 13(b)]. The dynamic density structure factor reveals a gap for long-wavelength excitations in both cases, see Figs. 13(c) and 13(d). Finally, the dynamic spin structure factor in the Mott phase [Fig. 13(e)] has a gapless linear mode at small q , and enhanced spectral weight at $q = \pi = 2k_F$ reflecting the $1/r$ antiferromagnetic spin correlations. In the Peierls phase, Fig. 13(f), the weight at $q = \pi$ is suppressed, but the spin gap at $q = 0$ is much smaller than in Fig. 9(b).

V. DISCUSSION

A. Agreement of SSH and optical SSH models

Figure 1 reveals a remarkable quantitative agreement between results obtained for the SSH model (2) and the optical SSH model (3). We have found this agreement to hold for all parameters and observables considered. While theoretical arguments suggest that only the phonon frequency at $q = 2k_F$ is important for the low-energy physics of the SSH model [6, 16, 56], deviations may be expected at higher energies or smaller length scales, as typically probed in numerical simulations. However, for the parameter sets considered, the results are identical within error bars. This equivalence of the models (2) and (3) is consistent with the excellent agreement of the phase boundary for the optical SSH-UV model from quantum Monte Carlo simulations [25] and that obtained with the functional renormalization group [18] for the SSH-UV model with acoustic phonons. On the other hand, a significant shift of the critical value for the Mott-Peierls transition was reported in Ref. [31], although the values become almost identical for small U and V ; however, these results were obtained for a model

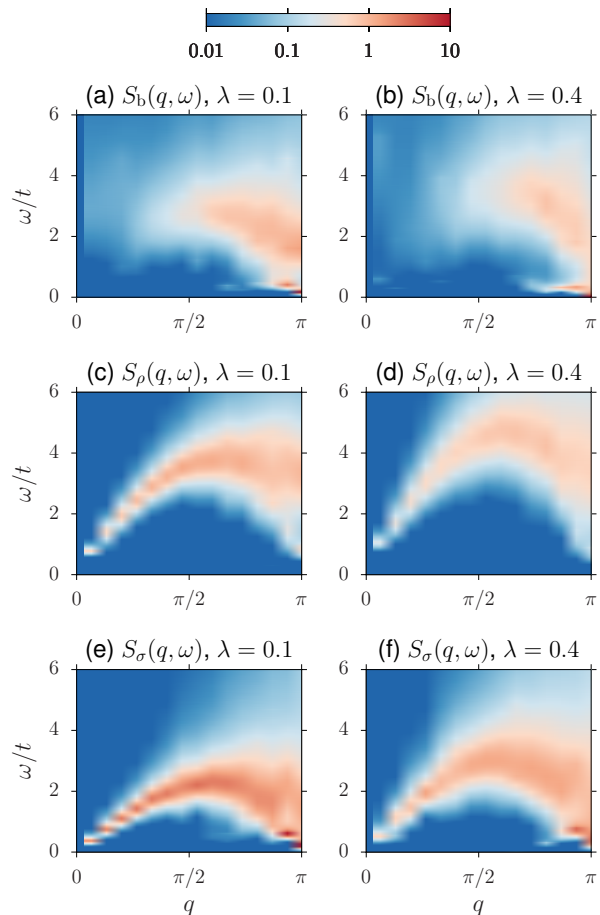


FIG. 13. (Color online) (a)–(b) Dynamic bond, (c)–(d) dynamic charge, and (e)–(f) dynamic spin structure factor of the optical SSH-UV model. Here, $\beta t = L = 30$, $\omega_0 = 0.5t$, $U = 2.5t$, and $V = 0.625t$.

with the original SSH coupling term. Therefore, the optical limit does not correspond to the optical SSH model considered here and in Ref. [25].

To understand the quantitative agreement between the SSH model and the optical SSH model, it is useful to consider the relation of the two models. The variables \hat{Q}_i of the SSH model (2) describe the longitudinal displacement of lattice site i from its original position. The hopping integral between sites i and $i+1$ depends on the length of the bond between these two sites, and hence on $\hat{Q}_{i+1} - \hat{Q}_i$. A change of \hat{Q}_i also changes the bond between sites i and $i-1$ because the lattice displacements at neighboring sites are coupled; this coupling gives rise to an acoustic phonon mode. In contrast, in the optical SSH model (3), the variables \hat{Q}_i describe the bond length itself, that is, they correspond to the difference $\hat{Q}_{i+1} - \hat{Q}_i$ in Eq. (2). Each of the L bonds is modeled as a harmonic oscillator with displacement \hat{Q}_i and momentum \hat{P}_i . Neighboring bonds are considered to be independent, as described by Einstein phonons. While the impact of this approximation is *a priori* unclear, our numerical results suggest that

both models give identical results.

We attribute the quantitative agreement to the fact that at half-filling ($2k_F = \pi$), the $2k_F$ bond correlations—generic for Luttinger liquids and Mott insulators [with a power-law decay as described by Eqs. (18) and (21)] as well as for Peierls insulators with long-range bond order—are equivalent to alternating displacements of neighboring bonds. Because of the inherent preference for $2k_F$ (alternating) bond correlations, it is not necessary to encode the anticorrelation between the lengths of neighboring bonds into the Hamiltonian. While the SSH and optical SSH models are not connected by a canonical transformation, a change to bond variables $\hat{q}_i = (\hat{Q}_{i+1} - \hat{Q}_i)/\sqrt{2}$ and conjugated bond momenta \hat{p}_i in Eq. (2) gives the optical SSH model (3) up to an additional term of the form $\sum_i \hat{p}_i \hat{p}_{i-1}$ responsible for the phonon dispersion. Neglecting this term amounts to replacing $\omega_q = \omega_\pi \sin(q/2)$ by $\omega_q = \omega_\pi$. Because $\sin(q/2)$ has a maximum at $q = \pi$, the first-order correction $\sim q$ vanishes for half-filling at the dominant value $q = 2k_F$ that determines the low-energy physics. From both arguments provided, we expect the models (2) and (3) to give different results away from half-filling where $2k_F \neq \pi$.

B. Lattice fluctuations and low-energy theory

The question of the impact of quantum lattice fluctuations on the dimerized Peierls state has been raised soon after the original work of SSH [6, 11, 12]. However, while (thermal or quantum) fluctuations are in principle expected to destroy long-range order for sufficiently weak electron-phonon interactions, the Peierls state remains stable at $T = 0$ in the spinful SSH model (although the dimerization is reduced), as confirmed by renormalization group methods [17, 18, 56, 61] and numerical simulations [6, 15, 25, 31]. In this respect, the SSH model is hence quite different from the Holstein model. In the latter, a metallic phase emerges from lattice fluctuations in both the spinless and the spinful case [19–21]. The spinful SSH model hence constitutes a case where Peierls' theorem is valid beyond the adiabatic limit.

For the SSH model, lattice fluctuations destroy long-range order if additional electron-electron interactions are taken into account [25, 31]. In this case, the critical value λ_c depends strongly on the phonon frequency [25]. However, a metallic state does not seem to exist. Instead, the phase diagram in the (λ, ω_0) plane for fixed large U reflects the physics of the Heisenberg spin-phonon model, which is always dimerized in the adiabatic limit, but has a gapless phase with critical spin correlations for $\omega_0 > 0$ and $\lambda < \lambda_c$ [25, 28, 62, 63]. For large U , this phase corresponds to the Mott phase of the SSH model.

The absence of a metallic phase in the spinful SSH model was also predicted from two-cutoff renormalization group calculations [17, 56, 61]. Because the forward scattering matrix element g_2 is exactly zero, any repulsive umklapp scattering g_3 is relevant. While this result

agrees with numerical results and the functional renormalization group, applications of the same method to the Holstein model [17, 56, 61] fail to describe the extended metallic phase at weak coupling. The two-cutoff renormalization group is hence not reliable in general. The likely reason why it gives correct results for the SSH model is that the physics of the latter at finite ω_0 is essentially the same as for $\omega_0 = \infty$ [6], so that retardation effects do not play a significant role.

While a purely fermionic theory is in general not sufficient to capture the physics of systems with a coupling to quantum phonons, a comparison with bosonization and renormalization group results for fermionic models provides valuable insights. Although the microscopic problem is rather different, the metal-insulator transition of the spinless SSH model can be related to a spinless Luttinger liquid that undergoes a Mott transition to a gapped $2k_F$ charge-density-wave phase. In fact, in the limit $\omega_0 = \infty$, the spinless SSH model maps to a model of spinless fermions with hopping t and nearest-neighbor repulsion $v = \lambda$, which exhibits a quantum phase transition from a Luttinger liquid to a charge-density-wave insulator at $v = 2t$ (corresponding to $K_\rho = 1/2$) [43]. Similarly, numerical results for the spinless Holstein model—for which a strong-coupling picture also leads to a model of spinless fermions with repulsion v —also support a metal-insulator transition at $K_\rho = 1/2$ [64].

The physics of the spinful SSH and SSH-UV models may be related to bosonization results for the extended Hubbard model with onsite interaction u and nearest-neighbor interaction v [44]. Here, u and v correspond to effective interactions that emerge from both electron-electron and electron-phonon interactions. For the case $U = V = 0$, the existence of spin and charge gaps for any $\lambda > 0$ may be related to the fact that for $u = 0$, umklapp and backscattering are relevant for any $v > 0$, giving rise to a fully gapped phase with long-range $2k_F$ charge correlations (rather than a bond-order wave as in the SSH model; for the extended Hubbard model, $2k_F$ bond correlations have the same exponent as $2k_F$ charge correlations but a vanishing prefactor [44]). On the other hand, the Mott-Peierls transition observed for nonzero Coulomb interactions U and V (with $U \gg V$) may be understood in terms of the extended Hubbard model with $u > 0$ and $v > 0$. For the latter, umklapp scattering is relevant for any $u > 0$ and gaps out the charge sector [44], while a transition to a spin-gapped $2k_F$ charge-density-wave phase takes place near $u = 2v$ [44]. The Mott phase with gapless spin excitations that exists for $u \gtrsim 2v$ is identical to the Mott phase observed for $\lambda < \lambda_c$ in the SSH-UV model, whereas the fully gapped charge-density-wave phase may be related to the dimerized Peierls phase. (For the extended Hubbard model at weak to intermediate couplings u and v , two independent transitions for the spin and charge excitations as well as an intermediate bond-ordered phase exist [51, 57, 65–68].)

Although a metallic phase is absent in the SSH model, we note that an extension of an argument by Voit for

charge-density-wave insulators [69] implies that a metallic phase with dominant bond correlations can only be realized in Luther-Emery liquids with a gap for spin excitations, because according to Eq. (21) spin and bond correlations decay with the same power-law exponent in a Luttinger liquid with $K_\sigma = 1$.

Although the bosonization results for the extended Hubbard model capture several key aspects of the SSH- UV model, the continuum field theory does not account for the spontaneous breaking of a discrete Ising Z_2 symmetry at the Peierls transition. Instead, it provides a theory of $U(1)$ charge and spin phase fields that can be pinned when umklapp and/or backscattering terms become relevant, leading to Kosterlitz-Thouless transitions and massive excitations but no long-range order. Accordingly, the Mott phase has a charge gap and critical spin correlations, but does not break any symmetries. In contrast, the Peierls phase is characterized by charge and spin gaps and a broken Ising symmetry reflected in the central peak visible in Fig. 13(b). The existence of a $U(1) \times Z_2$ symmetry in the continuum limit has recently been illustrated for the spinless Holstein model [48].

VI. SUMMARY

We used the CT-INT quantum Monte Carlo method to study SSH models with quantum phonons. First, we demonstrated that the original SSH model with acoustic phonons gives results that agree within statistical errors with those for the optical SSH model, a property that

can be related to the inherent tendency toward $2k_F$ bond correlations. Next, we studied the Peierls metal-insulator transition of the spinless SSH model in terms of real-space correlation functions and excitation spectra. The results are consistent with a Kosterlitz-Thouless quantum phase transition at a critical Luttinger parameter $K_\rho = 1/2$. The spectra reveal the expected Peierls gap, soliton signatures, and a central peak related to long-range order. In the spinful case, we confirmed the absence of a metallic phase by detecting a spin gap even at weak coupling, and by demonstrating a symmetry-related degeneracy of spin and charge correlations. The spectral functions reveal a gap for single-particle, charge and spin excitations, and a central peak. Finally, we studied the spinful SSH model with additional electron-electron interactions appropriate for polyacetylene. Our results are consistent with a phase transition from a Mott state with critical spin and bond correlations to a Peierls state with long-range bond order and exponential decay of all other correlation functions. Electron-electron repulsion was found to enhance bond correlations. In contrast to the Holstein-Hubbard model, we found no indications for metallic behavior.

ACKNOWLEDGMENTS

We are grateful to the Jülich Supercomputing Centre for computer time, and acknowledge financial support from the DFG Grants No. AS120/10-1 and Ho 4489/3-1 (FOR 1807). We thank S. Ejima for providing us with benchmark results, and C. Bourbonnais, H. Fehske, and E. Jeckelmann for helpful discussions.

-
- ¹ W. P. Su, J. R. Schrieffer, and A. J. Heeger, Phys. Rev. Lett. **42**, 1698 (1979).
² R. Jackiw and C. Rebbi, Phys. Rev. D **13**, 3398 (1976).
³ A. J. Heeger, S. Kivelson, J. R. Schrieffer, and W. P. Su, Rev. Mod. Phys. **60**, 781 (1988).
⁴ X.-L. Qi and S.-C. Zhang, Rev. Mod. Phys. **83**, 1057 (2011).
⁵ A. P. Schnyder, S. Ryu, A. Furusaki, and A. W. W. Ludwig, Phys. Rev. B **78**, 195125 (2008).
⁶ E. Fradkin and J. E. Hirsch, Phys. Rev. B **27**, 1680 (1983).
⁷ E. Jeckelmann, Phys. Rev. B **57**, 11838 (1998).
⁸ G. Barcza, W. Barford, F. Gebhard, and O. Legeza, Phys. Rev. B **87**, 245116 (2013).
⁹ K. Michielsen and H. de Raedt, Modern Physics Letters B **10**, 855 (1996).
¹⁰ W. Su, Solid State Communications **42**, 497 (1982).
¹¹ M. Nakahara and K. Maki, Phys. Rev. B **25**, 7789 (1982).
¹² D. Schmeltzer, R. Zeyher, and W. Hanke, Phys. Rev. B **33**, 5141 (1986).
¹³ A. Takahashi, Phys. Rev. B **54**, 7965 (1996).
¹⁴ W. Barford, R. J. Bursill, and M. Y. Lavrentiev, Phys. Rev. B **65**, 075107 (2002).
¹⁵ W. Barford and R. J. Bursill, Phys. Rev. B **73**, 045106 (2006).
¹⁶ G. T. Zimanyi, S. A. Kivelson, and A. Luther, Phys. Rev. Lett. **60**, 2089 (1988).
¹⁷ H. Bakrim and C. Bourbonnais, Phys. Rev. B **76**, 195115 (2007).
¹⁸ H. Bakrim and C. Bourbonnais, arXiv:1502.01981 (2015).
¹⁹ J. E. Hirsch and E. Fradkin, Phys. Rev. B **27**, 4302 (1983).
²⁰ R. J. Bursill, R. H. McKenzie, and C. J. Hamer, Phys. Rev. Lett. **80**, 5607 (1998).
²¹ E. Jeckelmann, C. Zhang, and S. R. White, Phys. Rev. B **60**, 7950 (1999).
²² D. Baeriswyl, D. Campbell, and S. Mazumdar, in *Conjugated Conducting Polymers*, Springer Series in Solid-State Sciences, Vol. 102, edited by H. Kiess (Springer Berlin Heidelberg, 1992) pp. 7–133.
²³ J. E. Hirsch, Phys. Rev. Lett. **51**, 296 (1983).
²⁴ J. Voit, Phys. Rev. Lett. **62**, 1053 (1989).
²⁵ P. Sengupta, A. W. Sandvik, and D. K. Campbell, Phys. Rev. B **67**, 245103 (2003).
²⁶ M. Hase, I. Terasaki, and K. Uchinokura, Phys. Rev. Lett. **70**, 3651 (1993).
²⁷ G. Wellein, H. Fehske, and A. P. Kampf, Phys. Rev. Lett. **81**, 3956 (1998).
²⁸ A. W. Sandvik and D. K. Campbell, Phys. Rev. Lett. **83**, 195 (1999).

- ²⁹ W. Barford, *Electronic and Optical Properties of Conjugated Polymers* (Oxford University Press, 2005).
- ³⁰ T. Holstein, Ann. Phys. (N.Y.) **8**, 325 (1959); **8**, 343 (1959).
- ³¹ C. J. Pearson, W. Barford, and R. J. Bursill, Phys. Rev. B **83**, 195105 (2011).
- ³² M. Capone, W. Stephan, and M. Grilli, Phys. Rev. B **56**, 4484 (1997).
- ³³ S. Barišić, J. Labbé, and J. Friedel, Phys. Rev. Lett. **25**, 919 (1970).
- ³⁴ S. Mazumdar and S. N. Dixit, Phys. Rev. Lett. **51**, 292 (1983).
- ³⁵ R. R. P. Singh and R. T. Scalettar, Phys. Rev. Lett. **66**, 3203 (1991).
- ³⁶ A. N. Rubtsov, V. V. Savkin, and A. I. Lichtenstein, Phys. Rev. B **72**, 035122 (2005).
- ³⁷ R. P. Feynman, Phys. Rev. **97**, 660 (1955).
- ³⁸ F. F. Assaad and T. C. Lang, Phys. Rev. B **76**, 035116 (2007).
- ³⁹ M. Hohenadler, S. Wessel, M. Daghofer, and F. F. Assaad, Phys. Rev. B **85**, 195115 (2012).
- ⁴⁰ K. S. D. Beach, arXiv:0403055 (2004).
- ⁴¹ J. Cardy, *Scaling and Renormalization in Statistical Physics* (Cambridge University Press, Cambridge, 1996).
- ⁴² J. Voit, Rep. Prog. Phys. **58**, 977 (1995).
- ⁴³ T. Giamarchi, *Quantum Physics in One Dimension* (Clarendon Press, Oxford, 2004).
- ⁴⁴ J. Voit, Phys. Rev. B **45**, 4027 (1992).
- ⁴⁵ M. Hohenadler, H. Fehske, and F. F. Assaad, Phys. Rev. B **83**, 115105 (2011).
- ⁴⁶ J. Voit, L. Perfetti, F. Zwick, H. Berger, G. Margaritondo, G. Grüner, H. Höchst, and M. Gioni, Science **290**, 501 (2000).
- ⁴⁷ A. Schneider et al., Gnuplot-colorbrewer: ColorBrewer color schemes for gnuplot. Zenodo. 10.5281/zenodo.10282.
- ⁴⁸ M. Weber, F. F. Assaad, and M. Hohenadler, Phys. Rev. B **91**, 235150 (2015).
- ⁴⁹ A divergent susceptibility is a necessary but not a sufficient condition for the existence of long-range order. In particular, a divergence occurs if the bond correlator in Eq. (19) decays with an exponent less or equal to one. Such a decay is characteristic of repulsive Luther-Emery liquids with a spin gap but without long-range order.
- ⁵⁰ S. Ejima, F. Gebhard, and S. Nishimoto, Phys. Rev. B **74**, 245110 (2006).
- ⁵¹ P. Sengupta, A. W. Sandvik, and D. K. Campbell, Phys. Rev. B **65**, 155113 (2002).
- ⁵² R. P. Hardikar and R. T. Clay, Phys. Rev. B **75**, 245103 (2007).
- ⁵³ A. Luther and V. J. Emery, Phys. Rev. Lett. **33**, 589 (1974).
- ⁵⁴ M. Hohenadler and F. F. Assaad, Phys. Rev. B **87**, 075149 (2013).
- ⁵⁵ M. Hohenadler, F. F. Assaad, and H. Fehske, Phys. Rev. Lett. **109**, 116407 (2012).
- ⁵⁶ L. G. Caron and C. Bourbonnais, Phys. Rev. B **29**, 4230 (1984).
- ⁵⁷ S. Ejima and S. Nishimoto, Phys. Rev. Lett. **99**, 216403 (2007).
- ⁵⁸ J. Voit, Journal of Physics C: Solid State Physics **21**, L1141 (1988).
- ⁵⁹ L. Balents and M. P. A. Fisher, Phys. Rev. B **53**, 12133 (1996).
- ⁶⁰ S. Kivelson and D. E. Heim, Phys. Rev. B **26**, 4278 (1982).
- ⁶¹ I. P. Bindloss, Phys. Rev. B **71**, 205113 (2005).
- ⁶² R. Citro, E. Orignac, and T. Giamarchi, Phys. Rev. B **72**, 024434 (2005).
- ⁶³ A. Weiße, G. Hager, A. R. Bishop, and H. Fehske, Phys. Rev. B **74**, 214426 (2006).
- ⁶⁴ S. Ejima and H. Fehske, Europhys. Lett. **87**, 27001 (2009).
- ⁶⁵ M. Nakamura, Journal of the Physical Society of Japan **68**, 3123 (1999).
- ⁶⁶ E. Jeckelmann, Phys. Rev. Lett. **89**, 236401 (2002).
- ⁶⁷ A. W. Sandvik, P. Sengupta, and D. K. Campbell, Phys. Rev. Lett. **91**, 089701 (2003).
- ⁶⁸ A. S. Sandvik, L. Balents, and D. K. Campbell, Phys. Rev. Lett. **92**, 236401 (2004).
- ⁶⁹ J. Voit, Eur. Phys. J. B **5**, 505 (1998).